# Ultimate soil resistance of the laterally loaded pile in uniform sand

Wang, H.; Wang, L. Z.; Askarinejad, A.; Hong, Y.; He, B.

**DOI**
10.1139/cgj-2021-0487

**Publication date**
2023

**Document Version**
Final published version

**Published in**
Canadian Geotechnical Journal

Canadian Geotechnical Journal

Note

# Ultimate soil resistance of the laterally loaded pile in uniform sand

**H. Wang**[a,c], **L. Z. Wang**[b], **A. Askarinejad**[a], **Y. Hong**[b], **and B. He**[d]

[a]Faculty of Civil Engineering and Geosciences, Delft University of Technology, 2628 CN, Delft, The Netherlands; [b]College of Civil Engineering and Architecture, Zhejiang University, 310027, Hangzhou, China; [c]Advanced Modelling Section, Department of Offshore Energy, Norwegian Geotechnical Institute, 0484, Oslo, Norway; [d]Key Laboratory for Far-shore Wind Power Technology of Zhejiang Province, Power China Huadong Engineering Corporation Limited, 311122, Hangzhou, China

Corresponding author: **H. Wang** (email: H.Wang-16@tudelft.nl)



## Abstract

Piles have been widely used as foundations to resist lateral loads. For the design of a laterally loaded pile, one of the most important inputs is the ultimate soil resistance ($p_{ult} = K_{ult}D\sigma'_v$, where $K_{ult}$ is the ultimate lateral soil resistance coefficient, $D$ is the pile diameter, and $\sigma'_v$ is the vertical effective stress). However, great discrepancy can be found in the existing design equations for piles in sand. To provide new insights and clarify the discrepancy in previous studies, in this study, a series of numerical simulations were performed on piles of different configurations using the finite element model validated by centrifuge pile tests. The computed results suggest that $K_{ult}$ is a function of depth ratios $z/D$ and $z/L$ for the flexible and rigid piles, respectively (where $z$ is the absolute depth and $L$ is the embedded pile length), and all existing design equations failed to reproduce the magnitude and distribution of $K_{ult}$. Additionally, the $K_{ult}$ of horizontally translated fixed-head rigid piles exhibits the same pattern as that of free-head flexible piles, suggesting that the difference between free-head flexible piles and rigid piles is caused by the change of failure modes.

**Key words:** ultimate soil resistance, sand, laterally loaded pile, finite element modelling, hypoplastic soil model

## 1. Introduction

The ultimate lateral soil resistance ($p_{ult} = K_{ult}D\sigma'_v$, where $K_{ult}$ is the ultimate lateral soil resistance coefficient, $D$ is the pile diameter, and $\sigma'_v$ is the vertical effective stress) of laterally loaded pile is an important input in pile design (Hajialilue-Bonab et al. 2013; Rathod et al. 2019, 2020, 2021). Although many design equations have been proposed (Brinch Hansen 1961; Broms 1964; Petrasovits and Award 1972; Reese et al. 1974; Fleming et al. 1992; Prasad and Chari 1999; Zhang et al. 2005; API 2014; Burd et al. 2020; Amar Bouzid 2021), as summarized in Table 1, significant discrepancy can be observed between the existing equations, regarding the distribution of $K_{ult}$ with depth ($z$) and the influence of pile diameter ($D$). In light of this, a series of numerical simulations using a validated finite element (FE) model were performed in this study to clarify the influence of pile diameter ($D$), aspect ratio ($L/D$), and failure mode on $K_{ult}$.

## 2. Finite-element modelling

All the FE analyses in this study were performed using the FE software Abaqus (Dassault Systèmes 2007). It should be noted that although the FE modelling is primarily used to calculate displacements, it has also been well used in a geotechnical context for ultimate limit state situations; for example, the study on retaining walls (Tom Wörden and Achmus 2013), pile foundations (Muraro et al. 2014, 2015; Burd et al. 2020), caisson foundation (Achmus et al. 2013), and shallow foundation (Pieczyńska-Kozłowska et al. 2015). Typical FE model mesh employed in all the analyses is presented in Fig. 1. Due to the symmetry of the problem, only half of the pile–soil system was modelled. In all the simulations, the sand and pile were modelled by eight-node linear strain brick elements (i.e., "C3D8"). The Coulomb interface model with a friction coefficient of $0.67\varphi$ ($\varphi$ is the critical state soil friction angle) was used to simulate the interface behaviour between the pile and soil (Achmus et al. 2020).

Many existing studies (Prasad and Chari 1999; Higgins et al. 2013; Klinkvort and Hededal 2014; Ahmed and Hawlader 2016; Hong et al. 2017) suggest that pile–soil interaction is strongly dependent on the failure mode of pile, i.e., the flexible or rigid response. Therefore, two series of simulations were performed first, where the piles are either fully flexible or rigid under free-head condition in each series. Three different diameters of 2, 4, and 6 m were investigated for the flexible piles in sand. The corresponding embedded pile lengths are 30, 60, and 60 m, which were designed to guarantee that the piles respond in flexible mode. For the rigid piles, four different diameters of 4, 6, 8, and 10 m but the

**Table 1.** Summary of existing design equations for the ultimate lateral soil resistance coefficient $K_{ult}$.

| No. | Reference | Pile type | Method | Equations |
|---|---|---|---|---|
| 1 | Brinch Hansen (1961) | Rigid pile | Analytical | *Arbitrary depth* (bounded by the $K^0_{\sigma'_v}$ at ground surface and $K^\infty_{\sigma'_v}$ at infinite depth):<br>$K_{ult} = \left(K^0_{\sigma'_v} + K^\infty_{\sigma'_v}\alpha\frac{z}{D}\right) / \left(1+\alpha\frac{z}{D}\right)$<br>$\alpha = \frac{K^0_{\sigma'_v}}{K^\infty_{\sigma'_v}-K^0_{\sigma'_v}} \frac{K_0 \sin\varphi}{\sin\left(45^\circ+\frac{12}{}\varphi\right)}$<br>*Ground surface* (difference between the active and passive coefficient of a horizontally translated rough wall):<br>$K^0_{\sigma'_v} =$<br>$e^{((1/2)\pi+\varphi)\tan\varphi}\cos\varphi\tan\left(45^o+\frac{12}{}\varphi\right) - e^{-((1/2)\pi-\varphi)\tan\varphi}\cos\varphi\tan\left(45^o-\frac{12}{}\varphi\right)$<br>*Infinite depth* (assuming a deep strip foundation under plane failure mechanism):<br>$K^\infty_{\sigma'_v} = N_c d K_0 \tan$<br>$N_c = \left[e^{\pi\tan\varphi}\tan^2\left(45^o+\frac{12}{}\varphi\right)-1\right]\cot\varphi$<br>$d = 1.58 + 4.09\tan^4\varphi$<br>$K_0 = 1 - \sin\varphi$<br>**Note:** $K_{ult}$ is the function of depth ratio ($z/D$) and equals to $K^\infty_{\sigma'_v}$ at infinite depth. |
| 2 | Broms (1964) | Not specified | Experimental and analytical | $K_{ult} = 3K_P$<br>$K_P = (1+\sin\varphi)/(1-\sin\varphi)$<br>**Note:** $K_{ult}$ is only a function of the soil friction angle ($\varphi$) and remains the same along the pile. |
| 3 | Petrasovits and Award (1972) | Not specified | Experimental | $K_{ult} = 3.7K_P - K_a$<br>$K_a = tan^2\left(45^o+\frac{1}{2}\varphi\right)$<br>**Note:** $K_{ult}$ is only a function of the soil friction angle ($\varphi$) and remains the same along the pile. |
| 4 | Reese et al. (1974) | Not specified | Experimental and analytical | *Shallow depth* (assuming a passive wedge-type failure mode):<br>$K_{ult} =$<br>$\left[\frac{K_0\frac{z}{D}\tan\varphi\sin\beta}{\tan(\beta-\varphi)\cos\alpha} + \frac{\tan\beta}{\tan(\beta-\varphi)}\left(1+\frac{z}{D}\tan\beta\tan\alpha\right) + K_0\frac{z}{D}\tan\beta\left(\tan\varphi\sin\beta-\tan\alpha\right) - K_a\right]$<br>*Deep depth* (assuming a lateral flow failure mode):<br>$K_{ult} = K_a\left(\tan^8\beta - 1\right) + K_0\tan\varphi\tan^4\beta$<br>$\alpha = \varphi/2$<br>$\beta = 45 + \varphi/2$<br>**Note:** $K_{ult}$ is dependent on the depth ratio ($z/D$) at shallow zone until reaching a critical value at deep zone, where it becomes only a function of the soil friction angle ($\varphi$). In addition, a constant value for $\alpha$ and $\beta$ was assumed defined by the soil friction angle ($\varphi$), while many studies (Kim et al. 2011; Hajialilue-Bonab et al. 2013; Yu et al. 2015) have found that the shape of wedge soil flow shape (i.e., $\alpha$ and $\beta$) changes with depth, pile deflection, and state of sand (loose or dense). The dilatancy of sand at different states (stress level at different depth for loose and dense of different mobilized strain levels at ultimate state) was not considered. For the deep lateral flow failure, the $\alpha$ was assumed to be zero, which is also questionable (Ashour et al. 1998; Hajialilue-Bonab et al. 2013). |
| 5 | Fleming et al. (1992) | Not specified | Experimental | $K_{ult} = K_P^2$<br>**Note:** $K_{ult}$ is only a function of the soil friction angle ($\varphi$) and remains the same along the pile. |
| 6 | Prasad and Chari (1999) | Rigid pile | Experimental | $K_{ult} = 10^{(1.3\tan\varphi + 0.3)}$<br>**Note:** $K_{ult}$ is only a function of the soil friction angle ($\varphi$) and remains the same along the pile. |
| 7 | Zhang et al. (2005) | Not specified | Empirical | $K_{ult} = 0.8K_P^2 + K_0\tan(\delta)$<br>**Note:** Since $\delta$ is usually a constant value related to soil friction angle for a pile in typical sand, $K_{ult}$ is only a function of the soil friction angle ($\varphi$) and remains the same along the pile. |
| 8 | Burd et al. (2020) | Numerical | | $K_{ult} = K_1 + K_2\frac{z}{L}$<br>$K_1 = 0.3667 + 25.89D_r$<br>$K_2 = 0.3375 - 8.900D_r$<br>**Note:** $K_{ult}$ varies with depth by the ratio with pile length ($z/L$) instead of pile diameter ($z/D$). This means that the value of $K_{ult}$ of different diameter ($D$) piles will be the same at the same depth ($z$) below the ground surface as long as the pile embedded length ($L$) is the same, despite the difference of the depth ratio $z/D$. |

**Table 1.** (*concluded*).

| No. | Reference | Pile type | Method | Equations |
|---|---|---|---|---|
| 9 | Amar Bouzid (2021) | | Analytical and numerical | *Shallow depth* (assuming a passive wedge-type failure mode): $K_{ult} = \left[\frac{K_0 \frac{z}{D} \tan\varphi \sin\beta}{\tan(\beta-\varphi)\cos\alpha} + \frac{\tan\beta}{\tan(\beta-\varphi)}\left(1 + \frac{z}{D}\tan\beta\tan\alpha\right) + K_0 \frac{z}{D}\tan\beta(\tan\varphi\sin\beta - \tan\alpha) - K_a\right]$ *Deep depth* (assuming a horizontally translated rigid disc in plane strain condition): $K_{ult} = \frac{12}{\pi}(K_P + K_0 \tan\delta)$ **Note:** the $K_{ult}$ for shallow depth is the same as that proposed by Reese et al. (1974). However, the $K_{ult}$ at deep depth was modified to have the similar form of that in Zhang et al. (2005). |

**Table 2.** Details of the numerical simulation programme.

| No. | Pile type | Relative density ($D_r$) | Diameter ($D$) | Embedded length ($L$) | Young's modulus ($E_{pile}$, GPa) | Aspect ratio ($L/D$) | Pile head condition |
|---|---|---|---|---|---|---|---|
| Series-1 | Flexible | 60% | 2 m | 30 m | 210 | 15 | Free |
| | Flexible | 60% | 4 m | 60 m | 210 | 15 | Free |
| | Flexible | 60% | 6 m | 60 m | 210 | 10 | Free |
| Series-2 | Rigid | 60% | 4 m | 30 m | – | 7.5 | Free |
| | Rigid | 60% | 6 m | 30 m | – | 5 | Free |
| | Rigid | 60% | 8 m | 30 m | – | 3.75 | Free |
| | Rigid | 60% | 10 m | 30 m | – | 3 | Free |
| Series-3 | Rigid | 60% | 4 m | 30 m | – | 7.5 | Fixed |
| | Rigid | 60% | 6 m | 30 m | – | 5 | Fixed |
| | Rigid | 60% | 8 m | 30 m | – | 3.75 | Fixed |
| | Rigid | 60% | 10 m | 30 m | – | 3 | Fixed |



same length of 30 m (i.e., $L/D$ = 7.5, 5, 3.75, 3) were studied. In addition, a third series of simulations was also performed on the rigid piles, but with a fixed head condition. This series of simulation was designed to explain the observed difference between the flexible and the rigid piles. Considering that the soil failure modes of fixed-head flexible pile are similar to that of the free head (i.e., wedge failure at shallow and flow around at deep zone), no further simulation was performed under this condition. The pile configurations were selected to cover the applications in existing and future offshore wind projects, i.e., $D > 6$ m and $L/D < 8$ (Negro et al. 2017; Wang et al. 2021*a*, *b*). The loading eccentricity is 5 m in all cases, since existing studies show that pile–soil interaction is not affected by the loading eccentricity (Klinkvort 2013; Wang et al. 2022). Details of the simulations are summarized in Table 2.

The hypoplastic model was used in this study to model the nonlinear, strain and stress history-dependent response of sand (von Wolffersdorff 1996; Niemunis and Herle 1997). The constitutive model has been implemented in Abaqus by the user-defined subroutine (Gudehus et al. 2008) and used in different applications (e.g., Ng et al. 2013). In this study, the model parameters (summarized in Table 3) for Toyoura sand were adopted, which have been calibrated against element test (Hong et al. 2016) and validated against centrifuge pile test in medium dense sand ($D_r$ = 65%) (Wang et al. 2021*a*, 2021*b*, 2022). Details about the sand, model calibration, and validation can be found in Ishihara (1993), Hong et al. (2016), and Wang et al. (2022).

**Fig. 1.** Typical finite element model mesh.

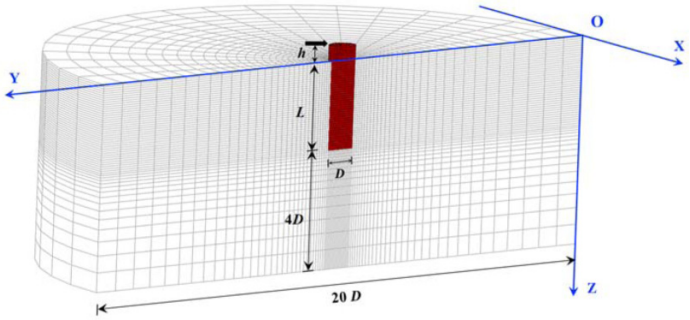


## 3. Interpretation of the computed results

In this section, the computed ultimate soil resistance of laterally loaded piles in sand has been presented and thoroughly discussed by comparing it with those calculated from the existing design equations. The computed soil resistance was obtained by differentiating the shear force profile extracted from the numerical model. The ultimate soil pressure ($p_{ult}$) is defined as the value in the flattened part of the $p$–$y$ curve.

### 3.1. Ultimate soil resistance of the flexible piles

Figure 2 presents the computed and calculated $K_{ult}$ profiles of flexible piles against the depth ($z$) normalized by the pile

**Table 3.** Calibrated parameters of hypoplastic model for Toyoura sand (Hong et al. 2016).

| | Description | Parameter | Values |
|---|---|---|---|
| Basic hypoplastic model (von Wolffersdorff 1996) | Effective angle of shearing resistance at critical state | $\varphi_c^{'}$ | 31 |
| | Hardness of granulates (kPa) | $h_s$ | $2.6 \times 10^6$ |
| | Exponent in the power law for proportional compression | $n$ | 0.27 |
| | Minimum void ratio at zero pressure | $e_{d0}$ | 0.61 |
| | Maximum void ratio at zero pressure | $e_{i0}$ | 1.1 |
| | Critical void ratio at zero pressure | $e_{c0}$ | 0.98 |
| | Exponent | $\alpha$ | 0.11 |
| | Exponent | $\beta$ | 4 |
| Intergranular strain concept (Niemunis and Herle 1997) | Parameter controlling initial shear modulus upon 180° strain path reversal | $m_R$ | 8 |
| | Parameter controlling initial shear modulus upon 90° strain path reversal | $m_T$ | 4 |
| | Size of elastic range | $R$ | $2 \times 10^{-5}$ |
| | Parameter controlling degradation rate of stiffness with strain | $\beta_r$ | 0.15 |
| | Parameter controlling degradation rate of stiffness with strain | $\chi$ | 1.0 |



**Fig. 2.** Comparison of computed ultimate soil resistance coefficients and those calculated from the existing design equations of different diameter free-head flexible piles (Note: a friction angle of 36° is used for the existing design equations).

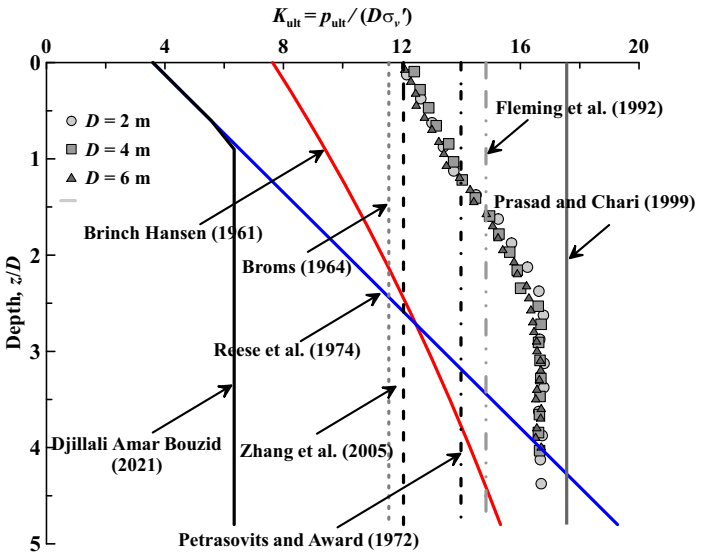


diameter ($D$), i.e., $z/D$. As shown in the figure, the $K_{ult}$ of different diameter piles is well unified when plotting against $z/D$. Similar to the theories in Brinch Hansen (1961), Reese et al. (1974), and Amar Bouzid (2021), the $K_{ult}$ exhibits the smallest value of 12 at ground surface and increase with $z/D$ until reaching the maximum value of 16.6 at a critical depth of 2.5 $D$. However, the predicted values of $K_{ult}$ at ground surface are 7.6, 3.6, and 3.6, and the critical depth is infinite, 17.7 $D$, and 0.9 $D$ for Brinch Hansen (1961), Reese et al. (1974), and Amar Bouzid (2021), respectively. Therefore, all of these three theories failed to predict the $K_{ult}$ of the flexible piles in sand. Meanwhile, the other theories, including Broms (1964), Petrasovits and Award (1972), Fleming et al. (1992), Prasad and Chari (1999), and Zhang et al. (2005), predicted constant values of $K_{ult}$ along the whole embedded length and did not account for the change of failure mechanism from shallow to deep zone. Therefore, it can be concluded that none of the existing theories can give accurate prediction of the ultimate soil resistance of the flexible piles in sand.

## 3.2. Ultimate soil resistance of the rigid piles

Figure 3 presents the computed and calculated $K_{ult}$ distribution of rigid piles against $z/D$ and $z/L$ ($L$ is the pile embedded length). As shown in Fig. 3*a*, the computed $K_{ult}$ profiles of different diameter piles change significantly with $z/D$, while all the existing design equations predict a single line. Among them, Brinch Hansen (1961), Reese et al. (1974), and Amar Bouzid (2021) defined $K_{ult}$ as a function of $z/D$, while Broms (1964), Petrasovits and Award (1972), Fleming et al. (1992), Prasad and Chari (1999), and Zhang et al. (2005) defined $K_{ult}$ to be independent of depth ($z$) or pile geometries (i.e., $D$, $L$, and $L/D$). However, none of the existing design equations can capture the magnitude and the distribution of $K_{ult}$. Instead, when plotting the results against $z/L$ in Fig. 3*b*, the computed $K_{ult}$ profiles converged at the same depth ratio $z/L$ independent of $D$ and $L/D$. This is also observed in Burd et al. (2020). Wang et al. (2020) explained that this is attributed to the rotation failure mechanism of the rigid piles under lateral loading. Therefore, it is clear that instead of being a function of $z/D$ as in Brinch Hansen (1961), Reese et al. (1974), and Amar Bouzid (2021) or being a constant value as in Broms (1964), Petrasovits and Award (1972), Fleming et al. (1992), Prasad and Chari (1999), and Zhang et al. (2005), the $K_{ult}$ of rigid piles in sand is a function of $z/L$. Among all the existing studies, Burd et al. (2020) is the only one defined in terms of $z/L$. However, as shown in Fig. 3*b*, the design equation in Burd et al. (2020) did not consider the change of failure mechanism with depth and requires further improvement.

**Fig. 3.** Comparison of the computed ultimate soil resistance coefficient $K_{ult}$ of free-head rigid piles with the existing design equations in terms of different depth ratios: (*a*) $z/D$ and (*b*) $z/L$ (Note: a friction angle of 36° is used for the existing design equations).

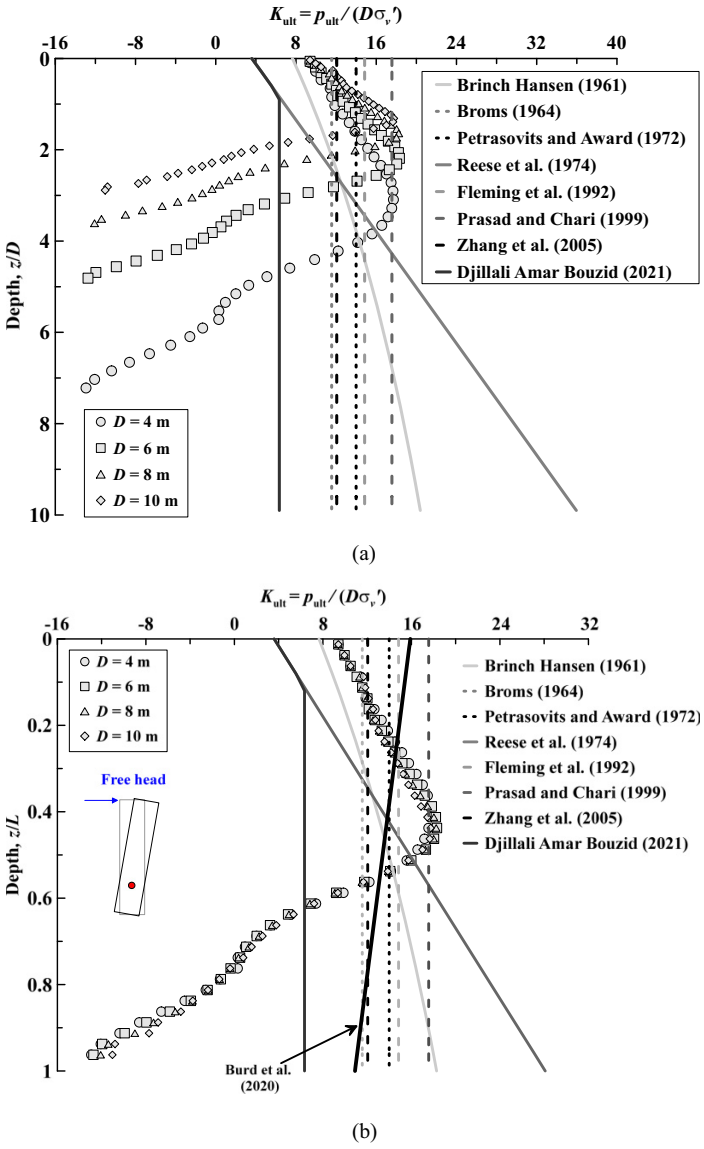


**Fig. 4.** The pile–soil interaction of horizontally translated piles under fixed head condition: (*a*) the $p_{ult}$ profiles and (*b*) the $K_{ult}$ profiles.

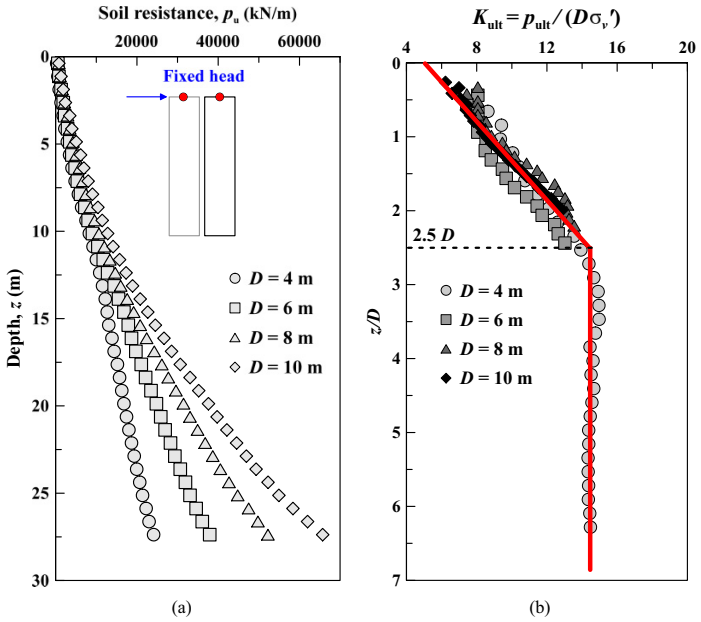


## 3.3. The influence of failure mode

In the preceding sections, the ultimate soil resistance of flexible and rigid piles in sand has been thoroughly investigated. It was found that the $K_{ult}$ of flexible pile is a function of $z/D$, while that of the rigid pile is a function of $z/L$. This difference is believed to be attributed to the different deflection modes of the laterally loaded piles. To clarify the reason for this difference, additional simulations on the rigid piles translated horizontally under a fixed-head condition were performed. Wang (2020) showed that the soil movement around the pile under rigid translation is similar to that of the flexible pile. As shown in Fig. 4*a*, the ultimate soil resistance increases with the depth and the pile diameter. However, when plotting $K_{ult}$ against $z/D$ in Fig. 4*b*, the diverged results in Fig. 4*a* converged perfectly into a single line. Similar to the response of flexible piles, the $K_{ult}$ of horizontally translated rigid piles increases at shallow depth from the smallest value at ground surface to a critical value at the depth of 2.5 $D$ and then remains the same for deeper zones. Therefore, it can be concluded that the different distributions of $K_{ult}$ against depth for flexible and rigid piles are attributed to the different failure modes (i.e., soil flow mode around the pile).

## 4. Conclusions

This study presents a thorough investigation on the ultimate soil resistance of the laterally loaded piles in sand through a series of numerical simulations on flexible and rigid piles using the well-validated FE model. Based on this study, the following conclusions can be drawn:

a) The $K_{ult}$ of flexible piles is a function of $z/D$, which exhibits the smallest value at the ground surface and then increases with depth until reaching the depth of 2.5 $D$, after which the value becomes constant.
b) Different from the dependency of $K_{ult}$ on $z/D$ for flexible piles, the $K_{ult}$ of free-head rigid piles is a function of $z/L$ due to the rotation failure mechanism.
c) The dependency of $K_{ult}$ on depth ratio ($z/D$ or $z/L$) is attributed to the soil failure modes of the piles. The free-head flexible piles and the horizontally translated fixed-head rigid piles exhibit the same distribution of $K_{ult}$ with depth, i.e., function of $z/D$, while that of free-head rigid pile is a function of depth ratio $z/L$.
d) None of the existing design equations can predict correctly the magnitude and distribution of $K_{ult}$ for both flexible and rigid piles in uniform sand.

## 5. Limitations

All the simulations in this study were performed in the uniform sand under drained condition using the hypoplastic model calibrated against the element and centrifuge tests of Toyoura sand. While the main conclusions concerning the diameter effect and the dependency of the ultimate soil resistance coefficient $K_{ult}$ on the failure modes (i.e., the distribution of $K_{ult}$ against depth ratio $z/D$ and $z/L$ for free-head flexible and rigid piles) are expected to be generally applicable, the exact values (e.g., the critical depth of 2.5 $D$ in Figs. 2 and 4) can vary for different sands and layered soil. In addition, the piles in this study are either fully flexible or fully rigid, while piles used in the field can be semi-rigid. Therefore, future studies should be performed to quantify the influence of pile rigidity, soil layering, and drainage condition.

## Article information

### History dates

Received: 27 August 2021
Accepted: 25 September 2022
Accepted manuscript online: 16 November 2022
Version of record online: 15 March 2023

### Copyright



### Data availability

The research data are in possession of the authors and can be accessed by contacting the authors.

## Author information

### Author ORCIDs

H. Wang https://orcid.org/0000-0002-9268-2293
A. Askarinejad https://orcid.org/0000-0002-7060-2141

### Competing interests

The authors declare there are no competing interests.

### Funding information

The authors gratefully acknowledge the financial supports provided by National Key Research and Development Program (2018YFE0109500), National Natural Science Foundation of China (51779221, 51909249, and 51939010), and Zhejiang Provincial Natural Science Foundation (LHZ20E090001 and LQ19E090001).

## References

Achmus, M., Akdag, C.T., and Thieken, K. 2013. Load-bearing behavior of suction bucket foundations in sand. Applied Ocean Research, **43**: 157–165. doi:10.1016/j.apor.2013.09.001.

Achmus, M., Schmoor, K.A., Herwig, V., and Matlock, B. 2020. Lateral bearing behaviour of vibro- and impact-driven large-diameter piles in dense sand. Geotechnik, **43**(3): 147–159. doi:10.1002/gete.202000006.

Ahmed, S.S., and Hawlader, B. 2016. Numerical analysis of large-diameter monopiles in dense sand supporting offshore wind turbines. International Journal of Geomechanics, **16**(5): 04016018. doi:10.1061/(ASCE)GM.1943-5622.0000633.

Amar Bouzid, D. 2021. Analytical quantification of ultimate resistance for sand flowing horizontally around monopile: new $p$– $y$ curve formulation. International Journal of Geomechanics, **21**(3): 04021007. doi:10.1061/(ASCE)GM.1943-5622.0001927.

American Petroleum Institute (API). 2014. Geotechnical and foundation design considerations. API RP 2GEO. API, Washington, DC.

Ashour, M., Norris, G., and Pilling, P. 1998. Lateral loading of a pile in layered soil using the strain wedge model. Journal of Geotechnical and Geo-environmental Engineering, **124**(4): 303–315. doi:10.1061/(ASCE)1090-0241(1998)124:4(303).

Brinch Hansen, J. 1961. The ultimate resistance of rigid piles against transversal forces. Bulletin 12. Danish Geotechnical Institute, Lyngby, Denmark. pp. 1–9.

Broms, B.B. 1964. Lateral resistance of piles in cohesionless soils. Journal of the Soil Mechanics and Foundations Division, **90**(3): 123–158. doi:10.1061/JSFEAQ.0000614.

Burd, H.J., Taborda, D.M., Zdravković, L., Abadie, C.N., Byrne, B.W., and Houlsby, G.T., 2020. PISA design model for monopiles for offshore wind turbines: application to a marine sand. Géotechnique, **70**(11): 1048–1066. doi:10.1680/jgeot.18.P.277.

Dassault Systèmes. 2007. ABAQUS 6.8 analysis user's manual. Simulia Corp., Providence, RI.

Fleming, W.K., Weltman, A.J., Randolph, M., and Elson, W.K. 1992. Piling engineering. CRC Press, Boca Raton, FL.

Gudehus, G., Amorosi, A., Gens, A., Herle, I., Kolymbas, D., Mašín, D., et al. 2008. The soilmodels. Info project. International Journal for Numerical and Analytical Methods in Geomechanics, **32**(12): 1571–1572. doi:10.1002/nag.675.

Hajialilue-Bonab, M., Sojoudi, Y., and Puppala, A.J. 2013. Study of strain wedge parameters for laterally loaded piles. International Journal of Geomechanics, **13**(2): 143–152. doi:10.1061/(ASCE)GM.1943-5622.0000186.

Higgins, W., Vasquez, C., Basu, D., and Griffiths, D.V. 2013. Elastic solutions for laterally loaded piles. Journal of Geotechnical and Geoenvironmental Engineering, **139**(7): 1096–1103. doi:10.1061/(ASCE)GT.1943-5606.0000828.

Hong, Y., Koo, C.H., Zhou, C., Ng, C.W., and Wang, L.Z. 2016. Small strain path-dependent stiffness of Toyoura sand: laboratory measurement and numerical implementation. International Journal of Geomechanics, **17**(1): 04016036. doi:10.1061/(ASCE)GM.1943-5622.0000664.

Hong, Y., He, B., Wang, L.Z., Wang, Z., Ng, C.W.W., and Mašín, D. 2017. Cyclic lateral response and failure mechanisms of semi-rigid pile in soft clay: centrifuge tests and numerical modelling. Canadian Geotechnical Journal, **54**(6): 806–824. doi:10.1139/cgj-2016-0356.

Ishihara, K. 1993. Liquefaction and flow failure during earthquakes. Geotechnique, **43**(3): 351–451. doi:10.1680/geot.1993.43.3.351.

Kim, Y., Jeong, S., and Lee, S. 2011. Wedge failure analysis of soil resistance on laterally loaded piles in clay. Journal of Geotechnical and Geo-environmental Engineering, **137**(7): 678–694. doi:10.1061/(ASCE)GT.1943-5606.0000481.

Klinkvort, R.T. 2013. Centrifuge modelling of drained lateral pile–soil response: application for offshore wind turbine support structures. Ph.D. thesis, Technical University of Denmark, Kongens Lyngby, Denmark.

Klinkvort, R.T., and Hededal, O. 2014. Effect of load eccentricity and stress level on monopile support for offshore wind turbines. Canadian Geotechnical Journal, **51**(9): 966–974. doi:10.1139/cgj-2013-0475.

Muraro, S., Madaschi, A., and Gajo, A. 2014. On the reliability of 3D numerical analyses on passive piles used for slope stabilisation in frictional soils. Géotechnique, **64**(6): 486–492. doi:10.1680/geot.13.T.016.

Muraro, S., Madaschi, A., and Gajo, A. 2015. Passive soil pressure on sloping ground and design of retaining structures for slope stabilisation. Géotechnique, **65**(6): 507–516. doi:10.1680/geot.14.P.211.

Negro, V., López-Gutiérrez, J.S., Esteban, M.D., Alberdi, P., Imaz, M., and Serraclara, J.M. 2017. Monopiles in offshore wind: preliminary estimate of main dimensions. Ocean Engineering, **133**: 253–261. doi:10.1016/j.oceaneng.2017.02.011.

Ng, C.W., Shi, J., and Hong, Y. 2013. Three-dimensional centrifuge modelling of basement excavation effects on an existing tunnel in dry

sand. Canadian Geotechnical Journal, **50**(8): 874–888. doi:10.1139/cgj-2012-0423.

Niemunis, A., and Herle, I. 1997. Hypoplastic model for cohesionless soils with elastic strain range. Mechanics of Cohesive-Frictional Materials: An International Journal on Experiments, Modelling and Computation of Materials and Structures, **2**(4): 279–299. doi:10.1002/(SICI)1099-1484(199710)2:4%3c279::AID-CFM29%3e3.0.CO;2-8.

Petrasovits, G., and Award, A. 1972. Ultimate lateral resistance of a rigid pile in cohesionless soil. In Proceedings of 5th European Conference on Soil Mechanics and Foundation Engineering, Madrid. Vol. **3**. pp. 407–412.

Pieczyńska-Kozłowska, J.M., Puła, W., Griffiths, D.V., and Fenton, G.A. 2015. Influence of embedment, self-weight and anisotropy on bearing capacity reliability using the random finite element method. Computers and Geotechnics, **67**: 229–238. doi:10.1016/j.compgeo.2015.02.013.

Prasad, Y.V., and Chari, T.R. 1999. Lateral capacity of model rigid piles in cohesionless soils. Soils and Foundations, **39**(2): 21–29. doi:10.3208/sandf.39.2_21.

Rathod, D., Muthukkumaran, K., and Thallak, S.G. 2019. Experimental investigation on behavior of a laterally loaded single pile located on sloping ground. International Journal of Geomechanics, **19**(5): 04019021. doi:10.1061/(ASCE)GM.1943-5622.0001381.

Rathod, D., Krishnanunni, K.T., and Nigitha, D. 2020. A review on conventional and innovative pile system for offshore wind turbines. Geotechnical and Geological Engineering, **38**(4): 3385–3402. doi:10.1007/s10706-020-01254-0.

Rathod, D., Nigitha, D., and Krishnanunni, K.T. 2021. Experimental investigation of the behavior of monopile under asymmetric two-way cyclic lateral loads. International Journal of Geomechanics, **21**(3): 06021001. doi:10.1061/(ASCE)GM.1943-5622.0001920.

Reese, L.C., Cox, W.R., and Koop, F.D. 1974. Analysis of laterally loaded piles in sand. In Offshore technology in civil engineering: hall of fame papers from the early years. pp. 95–105.

Tom Wörden, F., and Achmus, M. 2013. Numerical modeling of three-dimensional active earth pressure acting on rigid walls. Computers and Geotechnics, **51**: 83–90. doi:10.1016/j.compgeo.2013.02.004.

Von Wolffersdorff, P.A. 1996. A hypoplastic relation for granular materials with a predefined limit state surface. Mechanics of Cohesive-Frictional Materials: An International Journal on Experiments, Modelling and Computation of Materials and Structures, **1**(3): 251–271.

Wang, H. 2020. Lateral behaviour of offshore monopile and bucket foundations in sand. Ph.D. thesis, Zhejiang University, China.

Wang, H., Lehane, B.M., Bransby, M.F., Wang, L.Z., and Hong, Y. 2020. A simple approach for predicting the ultimate lateral capacity of a rigid pile in sand. Géotechnique Letters, **10**(3): 429–435. doi:10.1680/jgele.20.00006.

Wang, H., Wang, L., Hong, Y., Askarinejad, A., He, B., and Pan, H. 2021a. Influence of pile diameter and aspect ratio on the lateral response of monopiles in sand with different relative densities. Journal of Marine Science and Engineering, **9**(6): 618. doi:10.3390/jmse9060618.

Wang, H., Wang, L., Hong, Y., Mašín, D., Li, W., He, B., and Pan, H. 2021b. Centrifuge testing on monotonic and cyclic lateral behavior of large-diameter slender piles in sand. Ocean Engineering, **226**: 108299. doi:10.1016/j.oceaneng.2020.108299.

Wang, H., Fraser Bransby, M., Lehane, B.M., Wang, L., and Hong, Y. 2022. Numerical investigation of the monotonic drained lateral behaviour of large diameter rigid piles in medium dense uniform sand. Géotechnique, 1–39.

Yu, J., Huang, M., and Zhang, C. 2015. Three-dimensional upper-bound analysis for ultimate bearing capacity of laterally loaded rigid pile in undrained clay. Canadian Geotechnical Journal, **52**(11): 1775–1790. doi:10.1139/cgj-2014-0390.

Zhang, L., Silva, F., and Grismala, R. 2005. Ultimate lateral resistance to piles in cohesionless soils. Journal of Geotechnical and Geoenvironmental Engineering, **131**(1): 78–83. doi:10.1061/(ASCE)1090-0241(2005)131:1(78).